Isotopic composition of CO2 in the atmosphere of Mars: fractionation by diffusive separation observed by the ExoMars Trace Gas Orbiter

Juan Alday, Colin F. Wilson, Patrick G. J. Irwin, Alexander Trokhimovskiy, Franck Montmessin, Anna A. Fedorova, Denis A. Belyaev, Kevin S. Olsen, Oleg Korablev, Franck Lefèvre, et al.

JGR Planets

RESEARCH ARTICLE
10.1029/2021JE006992

Special Section:
ExoMars Trace Gas Orbiter - One Martian Year of Science

Isotopic Composition of CO_2 in the Atmosphere of Mars: Fractionation by Diffusive Separation Observed by the ExoMars Trace Gas Orbiter

Juan Alday[1], Colin F. Wilson[1], Patrick G. J. Irwin[1], Alexander Trokhimovskiy[2], Franck Montmessin[3], Anna A. Fedorova[2], Denis A. Belyaev[2], Kevin S. Olsen[1], O. Korablev[2], Franck Lefèvre[3], Ashwin S. Braude[3], Lucio Baggio[3], Andrey Patrakeev[2], and Alexey Shakun[2]

[1]AOPP, Department of Physics, University of Oxford, Oxford, UK, [2]Space Research Institute (IKI), Moscow, Russia, [3]LATMOS/CNRS, Guyancourt, France

Key Points:

- Isotopic ratios in CO_2 are observed to be consistent with telluric standards and to fractionate by diffusive separation above the homopause
- At least 20%–40% of the C reservoir has escaped to space throughout Martian history
- The higher $^{18}O/^{16}O$ ratio in H_2O than in CO_2 may be explained by a photochemical transfer of lighter O from H_2O to CO_2

Correspondence to:
J. Alday,
juan.aldayparejo@physics.ox.ac.uk

Citation:
Alday, J., Wilson, C. F., Irwin, P. G. J., Trokhimovskiy, A., Montmessin, F., Fedorova, A. A., et al. (2021). Isotopic composition of CO_2 in the atmosphere of Mars: Fractionation by diffusive separation observed by the ExoMars Trace Gas Orbiter. *Journal of Geophysical Research: Planets*, *126*, e2021JE006992. https://doi.org/10.1029/2021JE006992

Received 14 JUL 2021
Accepted 4 DEC 2021

Abstract

Isotopic ratios in atmospheric CO_2 are shaped by various processes throughout Mars' history, and can help understand what the atmosphere of early Mars was like to sustain liquid water on its surface. In this study, we monitor the O and C isotopic composition of CO_2 between 70 and 130 km for more than half a Martian year using solar occultation observations by the Atmospheric Chemistry Suite onboard the ExoMars Trace Gas Orbiter. We find the vertical trends of the isotopic ratios to be consistent with the expectations from diffusive separation above the homopause, with average values below this altitude being consistent with Earth-like fractionation ($\delta^{13}C = -3 \pm 37‰$; $\delta^{18}O = -29 \pm 38‰$; and $\delta^{17}O = -11 \pm 41‰$). Using these measurements, we estimate that at least 20%–40% of primordial C on Mars has escaped to space throughout history. The total amount of C lost from the atmosphere is likely to be well in excess of this lower limit, due to carbonate formation and further sink processes. In addition, we propose a photochemical transfer of light O from H_2O to CO_2 to explain the larger enrichment in the $^{18}O/^{16}O$ ratio in H_2O than in CO_2.

Plain Language Summary

There is ample evidence suggesting that liquid water was abundant on the surface of Mars in the past. However, climatic conditions on early Mars must have been very different from the ones we observe today to sustain liquid water on its surface. The ratios of the heavy and light isotopes in different species provide a very useful tool to estimate the early climate of Mars. In this study, we monitor the isotopic ratios of carbon dioxide in the atmosphere of Mars to provide more accurate estimates of these. With our measurements, and in context with previous studies, we estimate that at least 20%–40% of the carbon reservoir has been lost to space throughout Martian history. This, together with the sequestration of atmospheric C on the surface in the form of minerals, is consistent with the idea that the atmosphere of early Mars was denser than the one we observe today.

1. Introduction

Numerous pieces of mineralogical and geomorphological evidence suggest that liquid water was once abundant on the surface of Mars (e.g., Baker, 2001; Carr & Clow, 1981). The presence of large amounts of liquid water on the surface require climatic conditions very different from those resulting from the dry and thin atmosphere Mars has today. In fact, it is still not well understood how the past Martian atmosphere was able to produce sufficient greenhouse warming to sustain liquid water on the surface, nor what drove the transition of the climate to the one we observe today. Although, the composition of this early atmosphere remains unknown, carbon dioxide is thought to have been an important contributor to the total atmospheric pressure required to sustain liquid water on the surface, which later on migrated to non-atmospheric reservoirs in the surface or subsurface, or was lost to space (Ramirez et al., 2014; Wordsworth et al., 2013). Enrichment in the heavy isotopes of atmospheric species such as hydrogen, nitrogen or the noble gases with respect to Earth suggest that this transition was driven by the escape of a large portion of the atmosphere to space (e.g., Jakosky, 1997; Mahaffy et al., 2013; Owen et al., 1977). Isotope ratios can provide valuable constraints on the amount of atmosphere that existed in the past, but require a very detailed knowledge of the present-day isotopic ratios and the relative rates by which the different isotopologues of each species escape to space.

The isotopic composition of CO_2 in the atmosphere of Mars has been measured in several instances using both remote sensing and in situ techniques. Isotopic ratios are usually given as a deviation of the measured ratio R with respect to a standard R_s in units of per mil (e.g., $\delta^{13}C = (R/R_s - 1) \times 1{,}000$). The standard ratios representative of telluric values are defined by the Vienna Standard Mean Ocean Water (VSMOW) for oxygen ($^{18}O/^{16}O = 2{,}005.2 \times 10^{-6}$, $^{17}O/^{16}O = 379.9 \times 10^{-6}$), and the Vienna Pee Dee Belemnite (VPDB) for carbon ($^{13}C/^{12}C = 1.123 \times 10^{-2}$). Measurements made using the neutral mass spectrometers on the Viking aeroshell and landers revealed the oxygen and carbon isotope composition of Mars' atmosphere to be consistent with Earth within 5% (i.e., $\delta^{13}C = \delta^{18}O = 0 \pm 50‰$; Nier & McElroy, 1977; Owen, 1982). Early ground-based high resolution spectroscopic measurements revealed a possible depletion of the ratios in CO_2 with respect to Earth ($\delta^{13}C = -73 \pm 58‰$; $\delta^{18}O = -40 \pm 130‰$, Schrey et al. (1986); $\delta^{13}C = -73 \pm 58‰$; $\delta^{18}O = -130 \pm 80‰$, Krasnopolsky et al. (1996)), but more recent observations showed only marginal deviations with respect to the standard ($\delta^{13}C = 0 \pm 110‰$, Encrenaz et al. (2005); $\delta^{13}C = -22 \pm 20‰$; $\delta^{18}O = 18 \pm 18‰$, Krasnopolsky et al. (2007)). The most precise measurements of the C and O isotope composition in the Martian atmosphere were made by the Phoenix Lander and the Curiosity Rover, but observing two different values whose uncertainty ranges did not overlap. Niles et al. (2010) found carbon dioxide to be enriched in ^{18}O but not ^{13}C ($\delta^{13}C = -2.5 \pm 4.3‰$ and $\delta^{18}O = 31.0 \pm 5.7‰$) using measurements with the Thermal Evolved Gas Analyzer mass spectrometer on the Phoenix Lander. However, reconsideration of these data suggest that the lack of measured enrichment in ^{13}C may be a measurement artifact (Niles et al., 2014). On the other hand, Webster et al. (2013) reported similar enrichments in $\delta^{13}C$ and $\delta^{18}O$ ($\delta^{13}C = 46 \pm 4‰$ and $\delta^{18}O = 48 \pm 5‰$) using measurements made with the Sample Analysis at Mars' Tunable Laser Spectrometer (SAM/TLS) on the Curiosity Rover. The observed enrichment in $\delta^{13}C$ was confirmed by Mahaffy et al. (2013) using SAM's quadrupole mass spectrometer (SAM/QMS) ($\delta^{13}C = 45 \pm 12‰$).

The only evidence of variability in the isotope ratios of CO_2 was recently reported by Livengood et al. (2020) using ground-based spectroscopic observations, which revealed variations from $\delta^{18}O = -92 \pm 23‰$ to $\delta^{18}O = 71 \pm 18‰$ over a temperature increase from 266.9 to 275.4 K. The observed correlation between the oxygen isotopic ratios and the surface temperature could be indicative of fractionation during the adsorption of CO_2 on the Martian regolith (Livengood et al., 2020; Rahn & Eiler, 2001). The average isotopic ratio was reported to be consistent with Earth-like fractionation within the measured uncertainties ($\delta^{18}O = 9 \pm 14‰$), which stresses the need of understanding the variations of the isotopic ratios to disentangle the ratios representative of the whole atmospheric reservoir from those derived in localized measurements.

Because CO_2 is the major reservoir of C in the Martian atmosphere, the $^{13}C/^{12}C$ isotopic ratio in CO_2 can be used to estimate the escape of C through time. Hu et al. (2015) modeled the isotopic fractionation induced by atmospheric loss, outgassing and carbonate formation through time, analyzing the likelihood of different combinations of these to match the observed isotopic ratio in CO_2 at present, which is assumed to be the value reported from the measurements by the Curiosity Rover. This methodology suggests the presence of an early atmosphere with a surface pressure <1 bar, with denser atmospheric scenarios requiring large amounts of carbonate formation. Jakosky (2019) also estimated the fraction of the C reservoir lost to space throughout history, suggesting that this process could have removed 1–2 bars of CO_2. While these estimates are higher than those reported by Hu et al. (2015), Jakosky (2019) notes that this discrepancy can be explained by extrapolating the results to the same epoch (~4.3 billion years ago), where the results of Hu et al. (2015) would also indicate a loss of 1.0–1.7 bars of CO_2.

In this study, we monitor the C and O isotopic ratios in CO_2 in an altitude range of 70–130 km for more than half a Martian year (MY) using solar occultation observations made by the Atmospheric Chemistry Suite (ACS) onboard the ExoMars Trace Gas Orbiter (TGO). These measurements allow the determination of vertical profiles for each of the isotopic ratios, enabling the determination of altitude-dependant fractionation processes, and the estimation of the isotopic composition of CO_2 representative of the atmospheric reservoir outside of fractionation processes. In addition, we discuss the implications of our measurements to the evolution of CO_2 in the Martian atmosphere, as well as the implications of the different O isotopic ratios in H_2O and CO_2.

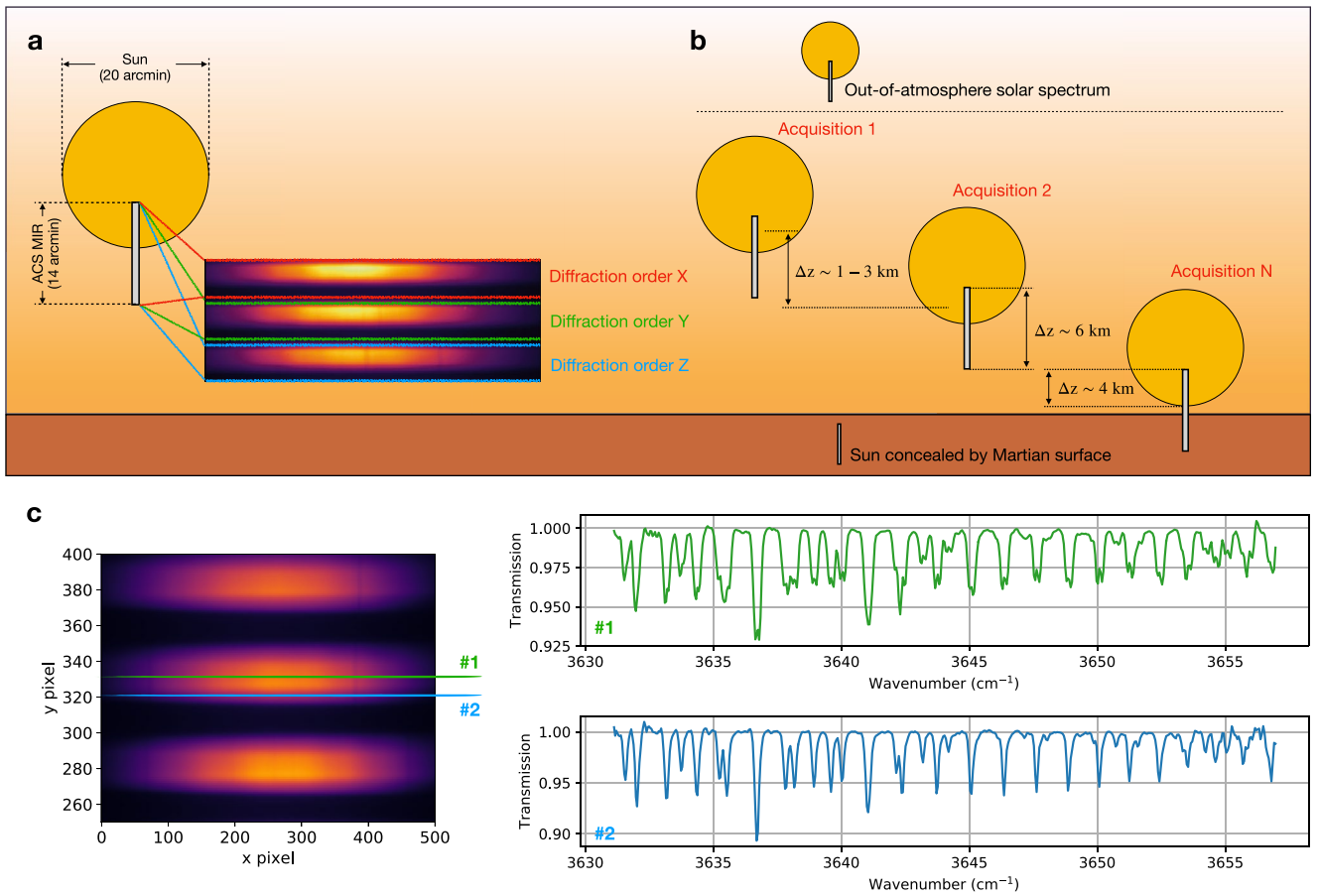

Figure 1. Illustration of the Atmospheric Chemistry Suite mid-infrared channel solar occultation observations. (a) In each acquisition, a number of diffraction orders are projected onto the detector frame. Since the slit is oriented perpendicularly to the surface of Mars, the width of each of the diffraction orders represents the instantaneous field-of-view of the instrument, with a vertical resolution of ~150 m/pixel. (b) During a solar occultation, several measurements are made at different tangent heights with a vertical resolution of ~1–3 km, although a finer vertical sampling can be achieved when making use of the instantaneous field-of-view in each of the acquisitions. (c) Selection of different rows within the detector frame from one acquisition allow the selection of different spectral ranges, if selecting rows from different diffraction orders, or different tangent altitudes, if selecting different rows from the same diffraction order. The green and blue lines highlight the difference in the instrument lineshape between the rows corresponding to maximum intensity (green) and the slit end (blue) for diffraction order 217.

2. ACS Solar Occultation Measurements

The ACS combines three infrared spectrometers covering a total spectral range of 0.7–17 μm (Korablev et al., 2018). The mid-infrared channel (MIR), used in this study, is an echelle cross-dispersion spectrometer dedicated to solar occultation measurements between 2.3 and 4.2 μm (2,380–4,350 cm^{-1}). To achieve high spectral resolution ($\lambda/\Delta\lambda \sim 30{,}000$) measurements in a broad instantaneous spectral range (0.15–0.3 μm) within the whole spectral range of the instrument, ACS MIR incorporates a movable secondary grating that allows the selection of diffraction orders. These diffraction orders are then projected along the vertical coordinate of a 640 × 512 pixel detector frame, while the horizontal coordinate contains the spectral information of the measurement. The width of the diffraction orders along the vertical coordinate expands ~20 pixels and represents the illuminated part of the slit (1 × 9 arcmin). Since the slit is oriented perpendicularly to the surface, the width of each diffraction order represents the instantaneous field-of-view of the instrument ($\Delta z \sim 4$ km at the tangent point), with a vertical resolution of approximately 150 m per pixel (see Figure 1a).

ACS MIR makes its measurements in the so-called solar occultation mode in which the Sun is continuously observed by the instrument from an altitude of 270 km until it is concealed by the Martian surface. The detector frames are recorded every 2.1 s, which allows the reconstruction of atmospheric vertical profiles with a resolution of 1–3 km, although a finer vertical sampling can be achieved by also making use of the instantaneous field-of-view of the instrument in each acquisition. The reference solar spectrum, used to derive the transmission spectra

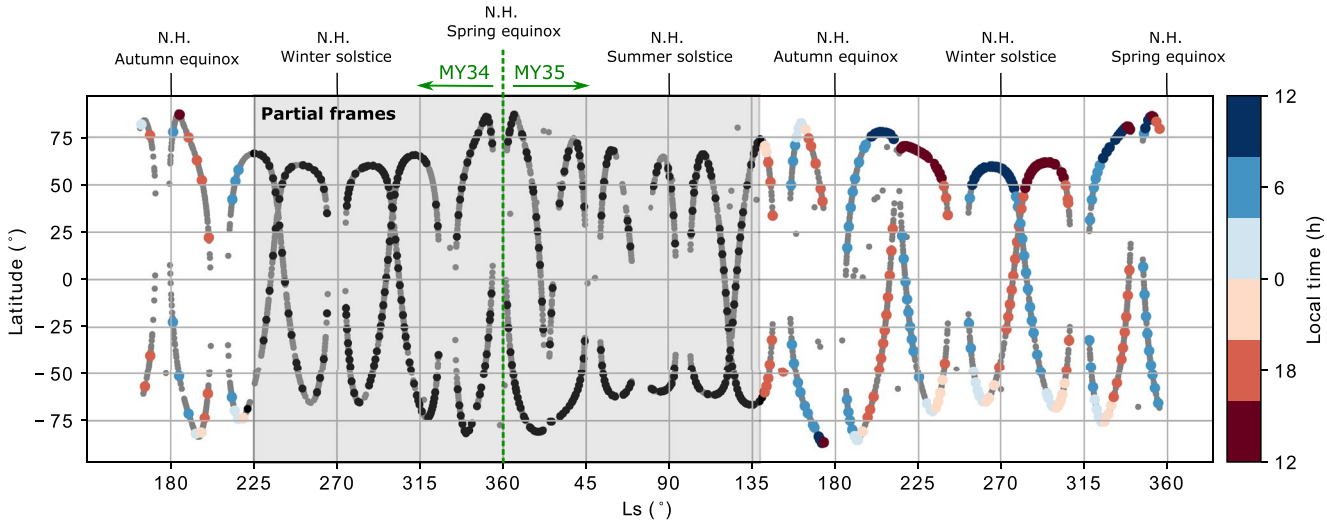

Figure 2. Observational coverage of Atmospheric Chemistry Suite (ACS) mid-infrared channel (MIR) full frame secondary grating position 4 solar occultation observations. Approximately 14% of all available ACS MIR observations between March 2018 and February 2021 (gray points) were made using secondary grating position 4 (black and colored points). During part of the science operations, observations were made using partial framing (black points within shaded region), which do not allow the derivation of the CO_2 isotopic ratios. The colored points, whose color represents the local time of the observations, are the full-frame observations, which allow the derivation of the CO_2 isotope ratios.

at each altitude, is calculated from the acquisitions above 190 km. On the other hand, the observations where the solar disk is concealed by the Martian surface are used to estimate the dark signal (see Figure 1b). Calibration of the spectra includes an orthorectification of the detector image, the removal of hot pixels, the dark signal and the straylight, and a correction for the sub-pixel drift occurring due to the slightly varying thermal state of the instrument. The spectral calibration of the measurements is performed by comparing the solar lines with the ACE-FTS solar atlas (Hase et al., 2010), and then further refined using atmospheric absorption lines of CO_2.

The instrument line shape (ILS) is impacted by an optical aberration in one of the lenses, causing a doubling of the detector image and consequently of the absorption lines. The impact of the doubling varies as a function of wavenumber and with detector row. This effect can be perceived from the spectra shown in Figure 1c: while the transmission spectrum taken from the slit end (blue line) shows single-peaked absorption lines, the spectrum from the center of the stripe (green line) is more affected by the doubling. The varying nature of the doubling effect requires it to be accounted for in the modeling of the observations. In this study, the ILS is parameterized using a double Gaussian function as described by Alday et al. (2019), in which the tuning parameters are fitted in parallel with the rest of the atmospheric properties. This approach has been validated against simultaneous solar occultation measurements of H_2O, CO, and CO_2 made by ACS NIR (Alday et al., 2019, 2021; Fedorova et al., 2020; Olsen et al., 2021).

The data set assembled for the analysis of the isotopic composition of CO_2 in this study comprises the observations made by ACS MIR using secondary grating position 4 from the start of the science operations in March 2018 to February 2021. This observing scheme enables the selection of 10 diffraction orders (215–224) in a spectral range between 2.65 and 2.78 μm (3,600–3,770 cm^{-1}), which encompass absorption bands of several isotopologues of CO_2 and of H_2O. In particular, the spectral region of interest for the measurement of the isotopic ratios in CO_2 lies in diffraction orders 217–219. During a substantial part of the science operations, ACS MIR observations made with secondary grating position 4 applied the so-called partial framing, in which just a portion of the detector frame was recorded and sent back to Earth. In these observations, diffraction orders 217–219 were not recorded, and impede the derivation of the isotopic ratios in CO_2. Therefore, the data set assembled for this study comprises the analysis of 246 full-frame observations, which are divided in two periods, one covering the range L_S = 164°–219° in MY34, and the second one covering the range L_S = 141°–356° in MY35, as shown in Figure 2.

3. Radiative Transfer Analysis

The radiative transfer analysis of the solar occultation measurements is made using the NEMESIS (Nonlinear optimal Estimator for MultivariatE spectral analySIS) algorithm (Irwin et al., 2008), which works using the optimal estimation formalism (Rodgers, 2000). In particular, five spectral windows within diffraction orders 217, 218, and 219 (3,634.8–3,645.7 cm^{-1}; 3,645.7–3,654 cm^{-1}; 3,652.5–3,662.5 cm^{-1}; 3,662.5–3,672 cm^{-1}; and 3,672–3,682 cm^{-1}) are selected to simultaneously retrieve the line-of-sight density of the four major isotopologues of CO_2 ($^{12}C^{16}O_2$, $^{13}C^{16}O_2$, $^{18}O^{12}C^{16}O$ and $^{17}O^{12}C^{16}O$), which allows the derivation of the $^{13}C/^{12}C$, $^{18}O/^{16}O$, and $^{17}O/^{16}O$ isotopic ratios. In addition, the parameters describing the ILS are also simultaneously fitted in each of the five spectral windows selected for the analysis of the observations.

All gaseous absorption in this work is modeled using pre-computed look-up tables calculated using line-by-line modeling. The spectroscopic parameters of the CO_2 absorption lines are taken from the 2016 version of the HITRAN database (Gordon et al., 2017), considering the pressure-broadening coefficients of the different isotopologues are given solely by self broadening. The partition functions, which determine the statistical properties of a gas in thermodynamic equilibrium at a given temperature and which are required to model the intensity of the spectral lines, are taken from Gamache et al. (2017). In the spectral range analyzed in this work, the strength of the CO_2 absorption lines is highly sensitive to the atmospheric temperature, which means that this parameter must be known to accurately model the spectra. The atmospheric temperature profile can be retrieved in this spectral range using the CO_2 absorption under the assumptions of a known CO_2 volume mixing ratio and an atmosphere in hydrostatic equilibrium (e.g., Quémerais et al., 2006). Such an approach, previously used for the derivation of the isotopic ratios in H_2O from ACS MIR spectra (Alday et al., 2019, 2021), requires the simultaneous retrieval of all tangent heights. While this methodology is optimal when using relatively narrow spectral windows, another method can be applied when using a broader spectral range. In particular, the rotational temperature of a particular gas can be retrieved by looking at the ratio of different spectral lines within an absorption band, which varies with temperature due to the different dependence to this parameter of the line strengths of each of the transitions (e.g., Mahieux et al., 2010; Olsen et al., 2016). This approach has the advantage of allowing the retrieval of the temperature field at each altitude level independently.

We develop a retrieval scheme to simultaneously constrain the rotational temperature of CO_2 along with the line-of-sight densities of the different isotopologues from each acquisition made by ACS MIR. To perform the retrieval of each acquisition independently and to allow a large number of spectral bands to be fitted simultaneously, we model the gaseous absorption of each transmission spectrum in a single homogeneous path with constant pressure and temperature. However, this assumption limits the vertical range under which this approach can be applied. In particular, the assumption of a constant pressure and temperature along the line of sight implies that all absorption occurs at the tangent point, with no contribution from the other atmospheric layers. The averaging kernels provide a measure of the sensitivity of the spectrum along the line of sight. Figure 3 shows the averaging kernels of the vertical profiles of the CO_2 isotopologues in our spectral range of interest. These kernels show that the sensitivity of the spectra below 40 km is extended and different for the several isotopologues, which can lead to biases when trying to determine the isotopic ratios. In contrast, the measurements above 60 km show a much narrower spread of the averaging kernels above the tangent height, which is similar for the different isotopologues. In particular, while 75% of the information is confined within 3 km above the tangent height for the measurements above 60 km, this number increases to 4 and 10 km for the measurements at 55 and 35 km, respectively. Based on these results, we only apply our retrieval scheme to the observations in the upper atmosphere (70–130 km), where the line-of-sight effects are expected to be minimal.

To evaluate the validity of the simultaneous retrieval of the rotational temperature and the line-of-sight densities of the different isotopologues, we perform a series of retrievals on a single spectrum assuming different pressures (10^{-5}-10^{-9} atm) and temperatures (100–225 K). The results of this test, summarized in Figure 4, show that there is a clear minimum of χ^2 at approximately 140 K, meaning that the rotational temperature can be simultaneously retrieved with the rest of the fitting parameters. On the other hand, changing the pressure over several orders of magnitude does not influence the level of agreement between the model and measurement, nor the other retrieved parameters. It is also shown in Figure 4 that, the retrieved isotopic ratios are highly sensitive to temperature, meaning that a small discrepancy in the temperature field yields a strong bias in the derived ratios, highlighting the importance of the simultaneous retrieval of the temperature field for an accurate estimation of the isotopic ratios in CO_2.

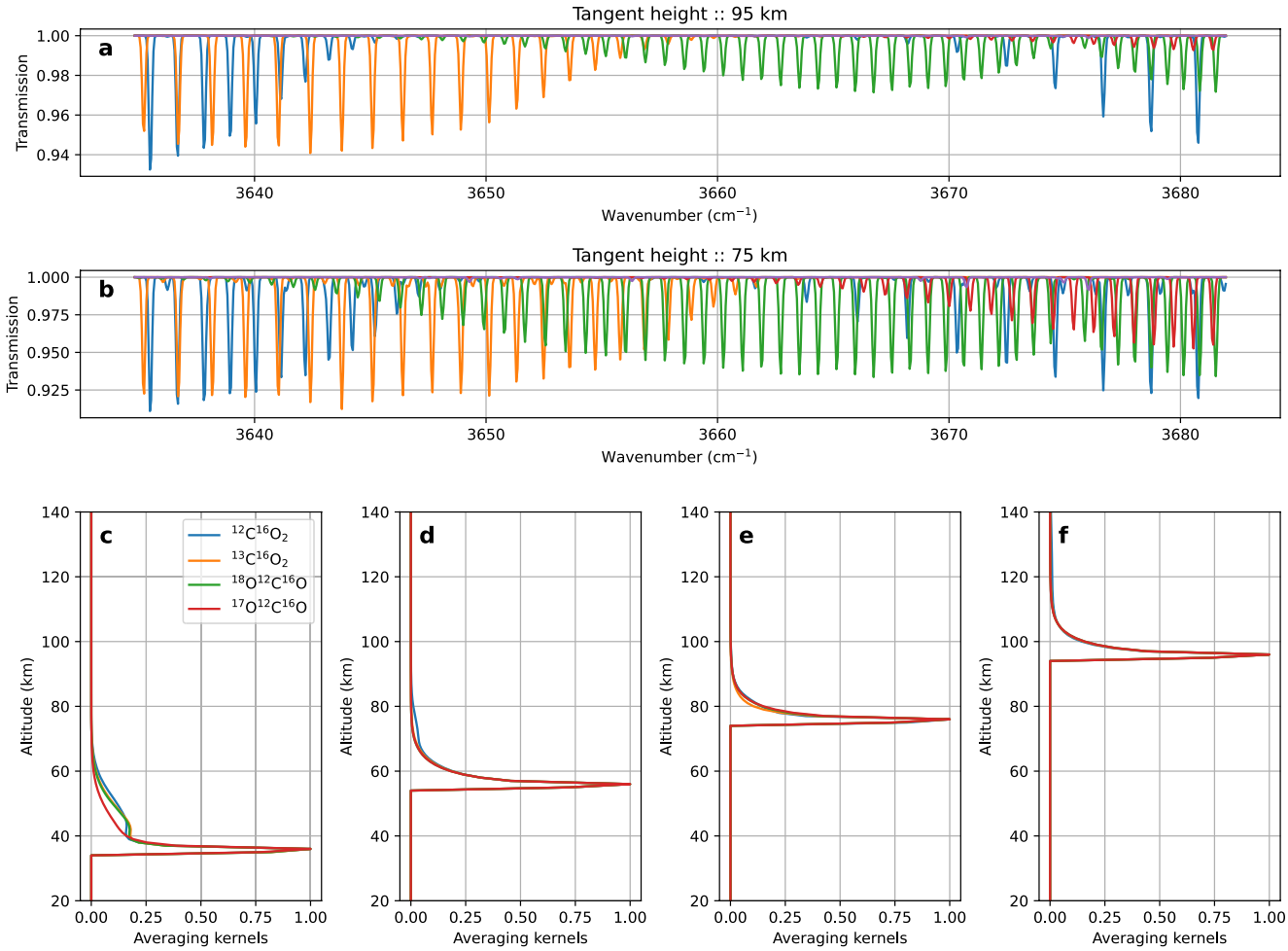

Figure 3. Sensitivity of the Atmospheric Chemistry Suite mid-infrared channel spectra along the line of sight. The top panels show two forward models at 95 (a) and 75 (b) km indicating the contribution of each isotopologue to the spectra. The bottom panels (c–f) show the normalized averaging kernels of the different isotopologues for a single measurement at tangent heights of 35, 55, 75, and 95 km, respectively. These kernels indicate that while below 70 km the contribution from layers above the tangent to the overall spectrum can be important and different for the several isotopologues, the kernels are narrower above 70 km and similar for the different isotopologues.

The developed retrieval scheme, including the simultaneous characterization of the rotational temperature, is applied independently to each acquisition made by ACS MIR above 70 km, which allows the derivation of the atmospheric temperature and the isotopic ratios at different altitudes above the Martian surface. To increase the confidence of the retrieved isotopic ratio profiles, we apply the developed scheme to six different rows from the detector, which are later combined by means of a weighted average, as shown in Figure 5. In particular, the procedure used to derive the vertical profiles is summarized as follows:

1. For each solar occultation measurement, select all ACS MIR acquisitions above 70 km and retrieve the atmospheric temperature along with the line-of-sight densities of $^{12}C^{16}O_2$, $^{13}C^{16}O_2$, $^{18}O^{12}C^{16}O$, and $^{17}O^{12}C^{16}O$.
2. The isotopic ratios and the corresponding uncertainties are determined given the uncertainties in the line-of-sight densities of the different isotopologues, following:

$$R = \frac{N_i}{N_1}, \tag{1}$$

$$\sigma_R = R \cdot \sqrt{\left(\frac{\sigma_{N_i}}{N_i}\right)^2 + \left(\frac{\sigma_{N_1}}{N_1}\right)^2}, \tag{2}$$

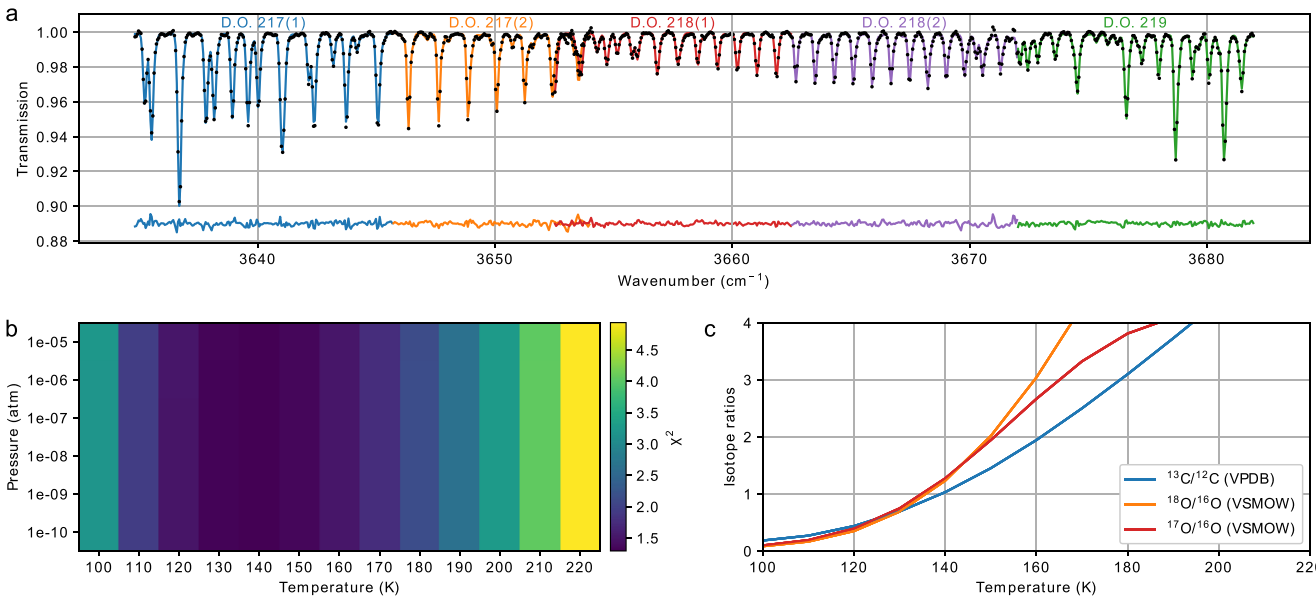

Figure 4. Sensitivity of the spectra and the derived isotopic ratios to the temperature. (a) Atmospheric Chemistry Suite mid-infrared channel spectrum at 100 km made during orbit 1,849 (black dots) and best fit to the data (colored lines) when assuming a temperature of $T = 140$ K. The residuals between the best fit and the measured spectrum are also shown, with the color of the lines highlighting the coverage of each of the spectral windows used for the retrieval. (b) Reduced χ^2 achieved for the different cases of pressure and temperature. (c) Derived isotopic ratios as a function of the assumed temperature.

where N_1 represents the line-of-sight density of $^{12}C^{16}O_2$, and N_i represents the line-of-sight density of the other isotopologues of CO_2.

3. Perform the retrieval and the derivation of the uncertainties introduced in the previous steps using six different detector rows, which allow the derivation of six vertical profiles for the atmospheric temperature and the isotopic ratios.
4. Combine the vertical profiles retrieved from each detector row by means of a weighted average given by,

$$\overline{\mu_j} = \frac{\sum_{i=1}^{6} \frac{x_{ij}}{\sigma_{ij}^2}}{\sum_{i=1}^{6} \frac{1}{\sigma_{ij}^2}}, \tag{3}$$

where μ_j is the averaged profile at the jth altitude level, and x_{ij} and σ_{ij}^2 are respectively the parameters (i.e., atmospheric temperature or isotopic ratios) and corresponding uncertainties derived for each detector row at each altitude level.

5. The uncertainties associated with the averaged profile are calculated using,

$$\overline{\sigma_j} = \mathrm{Max}\left(\overline{\sigma_1} = \sqrt{\frac{1}{\sum_{i=1}^{6} \frac{1}{\sigma_{ij}^2}}} \;;\; \overline{\sigma_2} = \sqrt{\frac{\sum_{i=1}^{6} \frac{(x_{ij}-\mu_j)^2}{\sigma_{ij}^2}}{\sum_{i=1}^{6} \frac{1}{\sigma_{ij}^2}}}\right), \tag{4}$$

where the first term represents the standard error on the mean, derived from the propagation of errors from each of the retrieved profiles from each detector row, and the second term represents the standard deviation of these profiles around the mean. We consider this method for calculating the uncertainties to provide a more accurate representation of the true uncertainty of the retrieval in which not only the random uncertainties, but also the systematic ones are captured (e.g., effect of the doubling of the absorption lines, since it impacts each row of the detector differently, or the effect of the temperature in the retrieval of the isotopic ratios, since the retrieval from each row yields slightly different temperatures at each level).

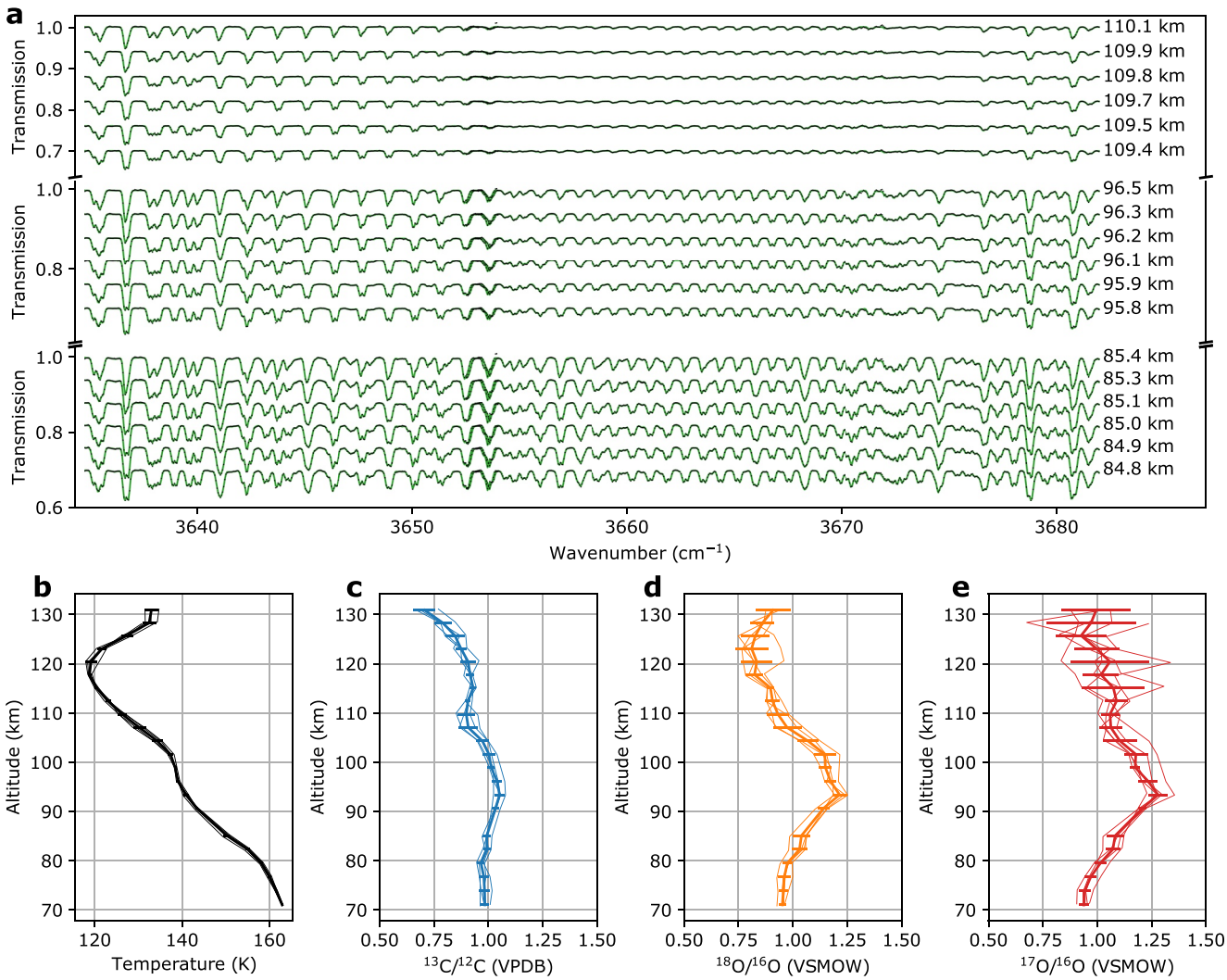

Figure 5. Example of Atmospheric Chemistry Suite (ACS) mid-infrared channel (MIR) spectra and summary of retrieval scheme. ACS MIR spectra shown in this figure (a) were obtained during the solar occultation in orbit 1,849 (Latitude = 82°, L_S = 163° in MY34, Local time = 3 hr). Retrievals of the rotational temperature (b) and the line-of-sight densities of $^{12}C^{16}O_2$, $^{13}C^{16}O_2$, $^{18}O^{12}C^{16}O$, and $^{17}O^{12}C^{16}O$ are performed independently using spectra from six different rows from the detector, which allow the derivation of the $^{13}C/^{12}C$ (c), $^{18}O/^{16}O$ (d), and $^{17}O/^{16}O$ (e) isotopic ratios. The retrieved profiles from each of the detector rows (thin lines) are later combined by means of a weighted average (thick lines). The increase in the $^{18}O/^{16}O$ and $^{17}O/^{16}O$ isotopic ratios is caused by a systematic bias in the retrieval scheme, which must be taken into account when analyzing the variations of the isotopic ratios.

To estimate the accuracy of the retrieval scheme, we perform a series of synthetic retrievals where the input isotopic ratios are known. These tests, explained more in-depth in Appendix A, reveal a very good accuracy of the retrievals of the $^{13}C/^{12}C$ ratio. On the other hand, these tests also reveal a bias in the retrieval of the O isotopic ratios: while the retrievals provide a good convergence at the lowermost altitudes (~70 km), the retrieved O isotope ratios are on average systematically higher (~0.05 VSMOW) than those used to generate the synthetic spectra near 100 km. This bias can lead to an unreal increase of the O isotope ratios with altitude, which must be taken into account when analyzing the retrieved ratios (see Figure 5 and Figure A1).

4. Results

The retrieval scheme introduced in the previous section is applied to all available secondary grating position 4 full-frame observations made by ACS MIR from March 2018 to February 2021 (see Figure 2). The results from this analysis are summarized in Figure 6, which shows the climatology of the retrieved atmospheric parameters. In the following subsections, these results are analyzed in more detail to highlight aspects of the data aiming to

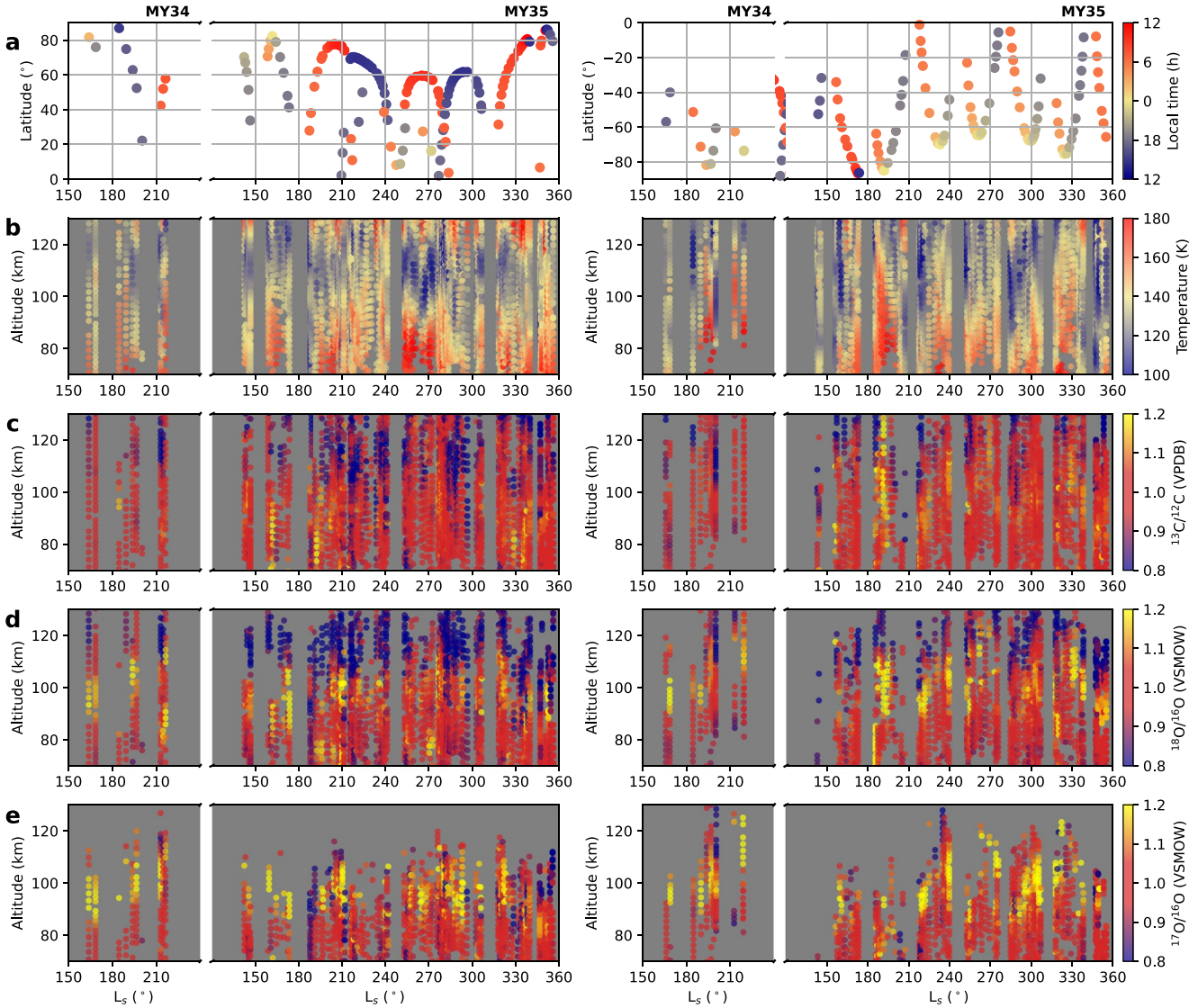

Figure 6. Climatology of the retrieved atmospheric parameters. The panels show the values of the retrieved parameters as a function of altitude and solar longitude for the northern (left) and southern (right) hemispheres. The panels in each of the rows represent the distribution of Atmospheric Chemistry Suite mid-infrared channel solar occultation observations, with the local time represented by the color bar (a), the atmospheric temperature (b), and the $^{13}C/^{12}C$ (c), $^{18}O/^{16}O$ (d), and $^{17}O/^{16}O$ (e) isotopic ratios with uncertainties lower than 0.075 Vienna Pee Dee Belemnite or Vienna Standard Mean Ocean Water. Most noticeable variations of the isotopic ratios are observed to occur as a function of altitude. To first order, no discernible patterns of variations are identified as a function of latitude, solar longitude or local time.

understand the variability of the isotopic ratios, the average values representative of the present-day atmosphere and the implications of these measurements to our understanding of the evolution of the Martian atmosphere throughout history.

4.1. Variability of the Isotopic Ratios

The evolution of the retrieved parameters with solar longitude in Figure 6 shows variations above the level of measured uncertainties, suggesting that these variations are not caused by the statistical error of the measurements, but by real processes in the atmosphere. We find the isotopic ratios to vary most noticeably as a function of altitude, showing repeatable patterns of variation throughout most of the observed period. Figure 7 shows the retrieved vertical profiles of temperature and the isotopic ratios measured in this data set, as well as the averaged profiles from these, which represent the altitude trends between 70 and 130 km. We identify two main features in

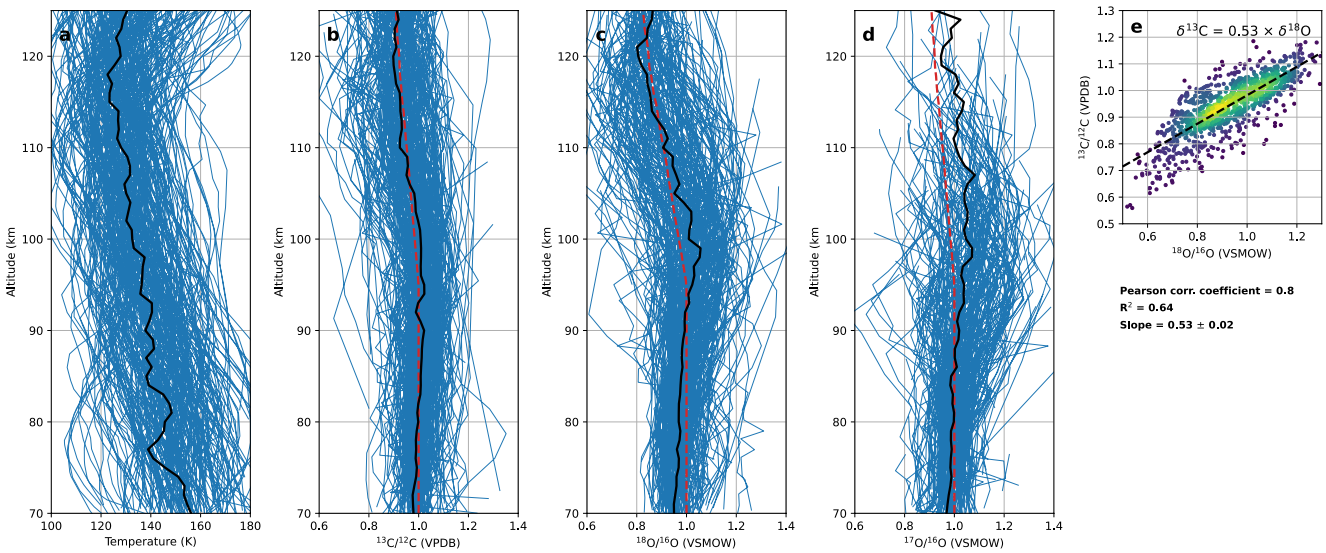

Figure 7. Heavy isotopes depleted with increasing altitude. The blue lines represent all measured vertical profiles of temperature (a), $^{13}C/^{12}C$ (b), $^{18}O/^{16}O$ (c), and $^{17}O/^{16}O$ (d) with uncertainties lower than 0.075 Vienna Pee Dee Belemnite and Vienna Standard Mean Ocean Water. Averaging these profiles allows the derivation of their altitude trends (black lines). The trends of the $^{18}O/^{16}O$ and $^{17}O/^{16}O$ isotopic ratios increase between 70 and 100 km, although this increase is caused by a systematic bias in the retrieval scheme. The trends of the $^{13}C/^{12}C$ and $^{18}O/^{16}O$ ratios show a decrease at the highest altitudes, consistent with the expectations of diffusive separation above the homopause altitude, which is located at $z_h = 95 \pm 2$ km. The correlation plot between the $^{13}C/^{12}C$ and $^{18}O/^{16}O$ ratios above 100 km (e) shows that the variations follow $\delta^{13}C \sim 0.5 \times \delta^{18}O$, consistent with the expectations from diffusive separation.

the altitude trends of the isotopic ratios: an increase in the O isotopic ratios from 70 to 100 km, and a decrease in the $^{13}C/^{12}C$ and $^{18}O/^{16}O$ isotopic ratios above ∼100 km.

The averaged profiles of the O isotopic ratios in Figure 7 show a significant increase from 0.9 to 1.0 VSMOW at 70–80 km, to 1.0–1.1 VSMOW at 95–105 km. This increase appears not to be followed by the $^{13}C/^{12}C$ isotopic ratio, which remains constant throughout this altitude range. An enrichment in the isotopic ratios of CO_2 could happen due to the difference in the ultraviolet photolysis cross-sections of the different isotopologues: the cross-sections of the heavy isotopes of carbon dioxide are smaller than those of the main isotopologue, which would therefore deplete the photolysis products in the heavy isotopes, leaving the unphotolysed CO_2 relatively enriched in these (Schmidt et al., 2013). However, based on the calculations by Schmidt et al. (2013), photolysis would preferentially enrich the $^{13}C/^{12}C$ ratio over both oxygen ratios, which is not what is inferred from the observations.

A systematic bias in the retrieved O isotopic ratios with altitude was identified while validating the retrieval scheme against synthetic spectra (see Appendix A). In particular, the retrieved O isotopic ratios were found to be increasingly overestimated with altitude, while the $^{13}C/^{12}C$ ratio was found to converge at all altitudes. This systematic bias, which is most likely caused by the simplified radiative transfer calculations used in this study, which assume a constant temperature along the path, is expected to occur in the ACS MIR observations too. Therefore, we conclude that the increase observed in the $^{18}O/^{16}O$ and $^{17}O/^{16}O$ is not caused by real fractionation, but by a systematic bias in the retrieval scheme.

The altitude trends of the isotopic ratios in Figure 7 also show a decrease of the $^{13}C/^{12}C$ and $^{18}O/^{16}O$ isotopic ratios above an altitude of approximately 100 km. Below this altitude, the isotopic ratios are found to be essentially consistent with Earth-like fractionation. In the case of the $^{17}O/^{16}O$ ratio, although the measurements below 100 km show a value consistent with Earth, there are fewer observations with low uncertainties above this altitude and the impact by the forementioned systematic bias keeps increasing with altitude, which makes it difficult to conclude if this isotopic ratio also decreases (see Figure A1). A decrease in the isotopic ratios at these altitudes follows the expectations from diffusive separation, which predict the density of each isotopologue to decrease according to their own mass-dependent scale heights above the homopause (e.g., Jakosky et al., 1994). The decrease of the isotopic ratios above the homopause due to diffusive separation is therefore established by the ratio of densities of the different isotopologues as a function of altitude and is given by,

$$R(z) = R_h \cdot \exp\left(\frac{-\Delta m \cdot g \cdot (z - z_h)}{k_B \cdot T}\right), \quad (5)$$

where R_h represents the isotopic ratio at the homopause, Δm is the mass difference between the two isotopologues (1 a.m.u for $^{13}C/^{12}C$ and $^{17}O/^{16}O$ and 2 a.m.u for $^{18}O/^{16}O$), g is the gravitational acceleration at the modeled altitude, z_h is the altitude of the homopause, k_B is Boltzmann's constant, and T is the temperature (e.g., Jakosky et al., 1994).

To estimate the homopause altitude z_h from the observations of the isotopic ratios, the model for diffusive separation in Equation 5 is fit to the averaged $^{13}C/^{12}C$ profile, using the measured temperature profile and assuming Earth-like fractionation below the homopause. The best fit, also displayed in Figure 7, shows a good agreement with the data, in which the retrieved homopause altitude was found to be $z_h = 95 \pm 2$ km. Slipski et al. (2018) monitored the altitude of the homopause in different seasons, local times and locations using the ratio of N_2 to Ar densities measured by NGIMS onboard the MAVEN spacecraft. These results show that the homopause is typically set at altitudes between 90 and 110 km, which agrees with the altitude at which we observe the fractionation.

While the altitude trend of the $^{18}O/^{16}O$ ratio also shows a decrease above ~100 km, it shows a poorer agreement with the model for diffusive separation, most likely due to the systematic bias mentioned before (see Figure 7c). Another way of unraveling the nature of the observed fractionation and test whether the decrease in the $^{13}C/^{12}C$ and $^{18}O/^{16}O$ ratios is caused by diffusive separation is to look at the correlation plots between these. Fractionation due to diffusive separation occurs because of the slightly different mass of the several isotopologues, which requires the variations of the isotope ratios to follow the expectations from mass-dependent fractionation (i.e., $\delta^{13}C \sim 0.5 \times \delta^{18}O$) (Young et al., 2002). Panel E on Figure 7 shows the correlation between the measured $^{13}C/^{12}C$ and $^{18}O/^{16}O$ ratios above 100 km, which show a positive linear correlation with a Pearson correlation coefficient of 0.8. To calculate the slope of the correlation we perform a linear regression which suggests that the measurements follow fractionation given by $\delta^{13}C = (0.53 \pm 0.02) \times \delta^{18}O$, which is in agreement with the expectations from mass-dependent fractionation. While the forementioned systematic bias is expected to produce an overestimation of the $^{18}O/^{16}O$ isotopic ratios, this is expected to be approximately constant in this altitude range, which does not affect the slope of the relation between $\delta^{13}C$ and $\delta^{18}O$. Therefore, we conclude that the observed decrease in the isotopic ratios is caused by diffusive separation of the different isotopologues above the homopause.

Apart from the variations of the isotopic ratios as a function of altitude, the ACS data set allows the analysis of potential seasonal and latitudinal variations. To first order, we find no differences in the behavior of the isotopic ratios as a function of latitude, season or local time, which show similar altitudinal patterns throughout most of the observed period. The altitude of the homopause varies as a function of L_S, latitude and local time, which will therefore produce variations of the minimum altitude at which the isotope ratios fractionate due to diffusive separation (Slipski et al., 2018). Similarly, Livengood et al. (2020) found variations of the $^{18}O/^{16}O$ ratio with local time and surface temperature, which appear to be caused by surface-atmosphere interactions. However, given the uncertainties of the derived profiles from this data set, we find no statistically significant differences between the profiles in both hemispheres, different local times, or in different periods of L_S.

4.2. Average Isotopic Ratios in the Present-Day Atmosphere

Estimations of the average isotopic ratios in CO_2 are essential for our understanding of the evolution of the atmosphere of Mars throughout history. Isotopic ratios inferred from localized measurements are subject to climatological processes that might affect the isotopic composition of the sample. To estimate the isotopic ratios representative of the Martian atmospheric reservoir, one must disentangle the values inferred from these measurements from potential sources of fractionation occurring in the atmosphere.

Figure 8 shows a histogram of the measured isotopic ratios in CO_2 as well as their corresponding uncertainties. The histograms are separated in three altitude regions (70–90, 90–110, and 110–130 km), which can be used to disentangle the points affected by fractionation (e.g., diffusive separation). The histograms show that most of the points with uncertainties lower than 75‰ correspond to the measurements between 70 and 90 km. The average values from the measurements made in this altitude range are $^{13}C/^{12}C = 0.997 \pm 0.037$ VPDB, $^{18}O/^{16}O = 0.971 \pm 0.038$ VSMOW and $^{17}O/^{16}O = 0.989 \pm 0.041$ VSMOW (i.e., $\delta^{13}C = -3 \pm 37$‰, $\delta^{18}O = -29 \pm 38$‰ and $\delta^{17}O = -11 \pm 41$‰), where the uncertainties correspond to the average measurement

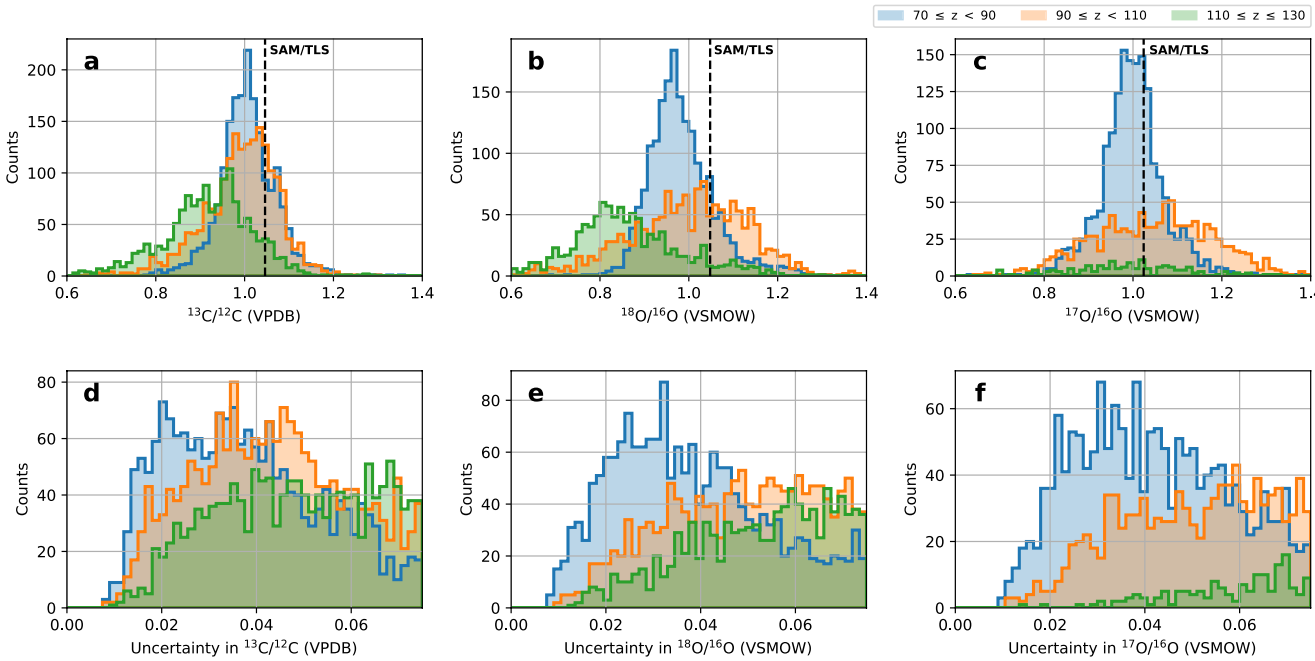

Figure 8. Histograms of the measured $^{13}C/^{12}C$ (a), $^{18}O/^{16}O$ (b) and $^{17}O/^{16}O$ (c) isotopic ratios and their retrieved uncertainties (d–f). The histograms for the different isotopic ratios are separated in three altitude regions (70–90 km – blue; 90–110 km – orange; 110–130 km – green) to highlight the variability of the vertical structure of the isotopic ratios. The black dashed lines in panels (a–c) represent the values of the isotopic ratios reported by Webster et al. (2013).

uncertainties (see Figure 8). While the measurements of $^{13}C/^{12}C$ between 90 and 110 km follow a distribution similar to that observed between 70 and 90 km, the measurements of $^{18}O/^{16}O$ and $^{17}O/^{16}O$ show more variability, partly caused by the greater typical uncertainties in this altitude range, and a higher mean value, caused by the systematic bias in the retrievals of these ratios, which tends to overestimate the isotopic ratios at these altitudes (see Figure A1). It must be noted that the histograms in the 70–90 km range might also include a slight overestimation of the O isotopic ratios due to this systematic bias. However, the variability of the slightly increasing trends of $^{18}O/^{16}O$ and $^{17}O/^{16}O$ in this altitude range are well covered by the reported uncertainties. Lastly, the measurements of the $^{13}C/^{12}C$ and $^{18}O/^{16}O$ isotopic ratios between 110 and 130 km depict values significantly smaller than those measured at lower altitudes due to the presence of fractionation above the homopause (see Figure 7).

Taking into account the accuracy of the retrievals and the variations of the isotopic ratios discussed in the previous sections, we consider the values measured in the lowest altitude range (70–90 km) to represent the average isotopic ratios representative of CO_2 in the atmosphere of Mars. These values may be compared with those reported in other studies (see Table 1). In particular, special attention is given to the comparison with the measurements from the Curiosity Rover (Webster et al., 2013), which show the lowest uncertainties and are often used as the isotopic ratios representative of the present-day Martian atmosphere in evolutionary models (Hu et al., 2015; Jakosky, 2019). The measurements of Webster et al. (2013) revealed an enrichment in the heavy isotopes of carbon dioxide with respect to Earth-like fractionation ($\delta^{13}C = 46 \pm 4‰$; $\delta^{18}O = 48 \pm 5‰$; and $\delta^{17}O = 24 \pm 5‰$). While these results are nominally consistent with our measurements, our derived average isotopic ratios do not show any evidence of enrichment in the heavy isotopes with respect to Earth.

One possible scenario to reconcile both measurements by SAM/TLS and ACS requires the presence of isotopic fractionation between the lower and upper atmospheres of Mars: while the Curiosity Rover measures the isotopic ratios on the surface, the analysis presented in this study is performed using observations between 70 and 130 km. However, it is not clear which processes could generate a depletion in the isotopic ratios between the lower and upper atmospheres of Mars. Condensation of CO_2 into ice clouds preferentially depletes the atmosphere in the heavy isotopes, although the magnitude of this depletion is expected to be small, especially for the carbon isotopic ratio, which may actually enrich the atmosphere in ^{13}C (Eiler et al., 2000). In addition, while formation of CO_2 ice clouds occurs sporadically in the atmosphere of Mars, the ACS measurements extend over a large range of

Table 1
Measured Isotope Ratios in CO_2 Compared to Previous Studies, Expressed as a Deviation With Respect to the VPDB and VSMOW Standards, Which Are Representative of Earth-Like Fractionation

Reference	Method	$\delta^{13}C$ (‰)	$\delta^{18}O$ (‰)	$\delta^{17}O$ (‰)
Schrey et al. (1986)	Earth-based	-73 ± 58	-37 ± 121	–
Owen (1982)	Viking Lander	-11 ± 55	-2 ± 50	–
Krasnopolsky et al. (1996)	Earth-based	-60 ± 150	-130 ± 80	–
Encrenaz et al. (2005)	Earth-based	0 ± 110	–	–
Krasnopolsky et al. (2007)	Earth-based	-22 ± 20	18 ± 18	–
Niles et al. (2010)	Phoenix Lander	-2.5 ± 4.3	31.0 ± 5.7	–
Webster et al. (2013)	Curiosity Rover	46 ± 4	48 ± 5	24 ± 5
Livengood et al. (2020)	Earth-based	–	9 ± 14	–
This study	ACS/TGO	-3 ± 37	-29 ± 38	-11 ± 41

Note. VPDB, Vienna Pee Dee Belemnite; VSMOW, Vienna Standard Mean Ocean Water.

latitudes, seasons and local times, which makes it unlikely that the isotopic ratios can be continuously fractionated by this mechanism. Another mechanism potentially depleting the isotopic ratios with altitude is the diffusive separation of the different isotopologues above the homopause, which is set at altitudes of approximately 100 km (see Figure 7 and Slipski et al. (2018)). However, our derivation of the average isotopic ratios is performed using measurements between 70 and 90 km, where diffusive separation is not expected to continuously fractionate the isotopic ratios.

Another possible scenario that might explain the differences between SAM/TLS and ACS lies on the impact of climatological isotopic fractionation in the derivation of the averaged isotopic ratios from both datasets. The ACS measurements extend over a large range of locations, seasons and local times, which allows averaging over hundreds of measurements, from which the effects of climatological fractionation are expected to be small. In that sense, although the measurements made by the Curiosity Rover are more precise, they were always made in the same location, at roughly the same local time, and covering only about 10% of a full MY. The contribution from seasonal cycling to these measurements is unknown, and so they might therefore not be representative of the whole atmospheric reservoir. In fact, Livengood et al. (2020) revealed high variability of the $^{18}O/^{16}O$ in the near-surface atmosphere, varying from $\delta^{18}O = -92 \pm 23$‰ to $\delta^{18}O = 71 \pm 18$‰ over a temperature increase from 266.9 to 275.4 K, which is most likely caused by surface-atmosphere interactions. On average, the measurements reported by Livengood et al. (2020) are essentially consistent with Earth-like fractionation (see Table 1). In addition, the values derived from different studies are in some cases inconsistent within the reported uncertainties, which might be indicative of isotopic fractionation in the atmosphere.

4.3. Implications to the Evolution of Mars' Atmosphere

Comparison between the primordial isotopic ratios and those in the present-day atmosphere allow the estimation of the amount of atmosphere lost to space throughout history. In particular, considering that CO_2 constitutes the major reservoir of C in the Martian atmosphere, the $^{13}C/^{12}C$ ratio allows the estimation of the amount of CO_2 lost to space assuming Rayleigh distillation, which is given by

$$R = R_0 \cdot x^{f-1}, \tag{6}$$

where R and R_0 represent the present-day and primordial $^{13}C/^{12}C$ ratio, respectively, x is the fraction of remaining atmosphere and f is the fractionation factor, which determines the efficiency of escape of the heavy isotope with respect to that of the lighter one. In particular, the fractionation factor is defined as,

$$f = \frac{\phi_{^{13}C}/\phi_{^{12}C}}{(^{13}C/^{12}C)_s}, \tag{7}$$

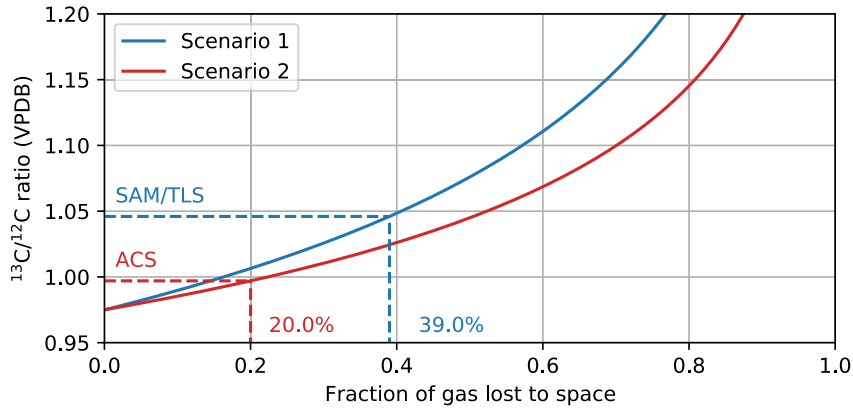

Figure 9. Estimation of the fraction of C lost to space throughout history from the $^{13}C/^{12}C$ isotopic ratio assuming Rayleigh distillation. In the first scenario, the isotopic composition of CO_2 is assumed to follow the measurements by SAM/TLS, but considering fractionation between the lower atmosphere and the homopause. In the second scenario, the isotopic composition of CO_2 is assumed to follow the measurements by Atmospheric Chemistry Suite, with no fractionation between the lower atmosphere and the homopause. In both scenarios the fractionation above the homopause is assumed to be caused by diffusive separation.

where $\phi_{^{12}C}$ and $\phi_{^{13}C}$ are the fluxes of escaping atoms of the two isotopologues, and $(^{13}C/^{12}C)_s$ is the isotopic ratio representative of the near-surface atmospheric reservoir.

Based on a primordial isotopic composition from measurements of magmatic carbon from Martian meteorites ($\delta^{13}C = -(20–30)‰$; Wright et al., 1986) and the isotopic composition of CO_2 in the present-day atmosphere measured by the Curiosity Rover ($\delta^{13}C = 46‰$; Webster et al., 2013), Jakosky (2019) estimated that at least 50% of the C reservoir has been lost to space throughout time. This estimation relies on the assumption that a substantial part of C was lost to space due to sputtering by pickup ions, where the fractionation factor is given by diffusive separation between the homopause and exobase altitudes (see Equation 1). Jakosky (2019) estimated the escape fractionation factor of $^{13}C/^{12}C$ using the analog factor derived by Jakosky et al. (2017) for the $^{38}Ar/^{36}Ar$ ratio using measurements from the MAVEN spacecraft, and re-scaling it taking into account the mass difference of 1 a.m.u for the C isotopes as compared to the 2 a.m.u for the isotopes of Ar. Based on these calculations, the average fractionation factor between the homopause and exobase altitudes due to diffusive separation is estimated to be $f_{h-e} \sim 0.9$. The main goal of this section is to apply the same approach as that of Jakosky (2019), but considering the implications of the $^{13}C/^{12}C$ measurements by ACS reported in this study. In particular, we consider the two suggested scenarios to reconcile the datasets between ACS and SAM/TLS.

In the first scenario, the difference between the average isotopic ratios derived from the ACS and SAM/TLS datasets implies a continuous source of fractionation between the isotopic ratios at the surface ($\delta^{13}C = 46‰$) and the homopause ($\delta^{13}C = -3‰$), which must be accounted for in the estimation of the fractionation factor. In particular, the net fractionation factor in this scenario is given by,

$$f = f_{s-h} \cdot f_{h-e}, \tag{8}$$

where f_{h-e} is the fractionation factor between the exobase and the homopause due to diffusive separation determined by Jakosky (2019) ($f_{h-e} \sim 0.9$) and f_{s-h} is the fractionation factor between the homopause and the surface ($f_{s-h} = (^{13}C/^{12}C)_h/(^{13}C/^{12}C)_s = 0.997/1.046 = 0.953$). Including this overall fractionation factor in the Rayleigh distillation equation (see Equation 6), and assuming that the isotopic ratio representative of the present-day atmosphere is that measured by the Curiosity Rover, we estimate that at least 40% of C in the Martian atmosphere has escaped to space throughout history (see Figure 9).

In the second scenario, we assume that the $^{13}C/^{12}C$ representative of the Martian atmospheric reservoir follows the value derived from the ACS data set. In this case, the enrichment in the heavy isotope with respect to the standard measured by Webster et al. (2013) is considered to be representative of the Martian atmosphere at a particular time and location impacted by climatological fractionation, but not representative of the atmospheric reservoir as a whole. Using the fractionation factor between the homopause and exobase altitudes due to diffusive separation

($f = f_{h-e} \sim 0.9$), we estimate that at least 20% of C in the Martian atmosphere has escaped to space throughout history (see Figure 9).

While these calculations provide a first-order estimate of the amount of C lost to space through time, a more accurate estimation of this quantity requires the combination of the several mechanisms by which C escapes to space and their corresponding fractionation factors. Early studies suggested the main source of C escape to be the dissociative recombination of CO^+ (McElroy, 1972), although further analyses revealed that it is the photodissociation of CO molecules that is the dominant process for the production of escaping C on Mars (Cui et al., 2019; Fox & Bakalian, 2001; Gröller et al., 2014). The escape fractionation factors by the photodissociation of CO (Hu et al., 2015) and the dissociative recombination of CO^+ (Fox & Hać, 1999) are lower than the fractionation factor induced by sputtering. In this case, the atmosphere would get more efficiently enriched in the heavy isotope as it escapes to space, indicating that a lower fraction of C would have been lost from the atmosphere of Mars through time. However, as noted by Jakosky (2019), the estimations performed in this study provide a lower limit on the amount of atmospheric escape, since other processes such as carbonate formation or outgassing of gas from the interior would result in a relative depletion of the heavy isotope in the atmosphere.

4.4. Relation Between the O Isotope Composition of H_2O and CO_2

Fractionation between the isotopic composition of H_2O and CO_2 will result if oxygen is exchanging between them. Therefore, examining the relative $\delta^{18}O$ can provide an insight on how these species interact with each other. The isotopic composition of H_2O in the Martian atmosphere was reported by Alday et al. (2021) using ACS MIR solar occultation observations also made with secondary grating position 4. This analysis revealed an average non-fractionated isotopic ratio of $^{18}O/^{16}O$ (H_2O) = 1.140 ± 0.080 VSMOW ($\delta^{18}O$ (H_2O) = 140 ± 80‰), which is therefore more enriched in the heavy isotope than that in CO_2 ($\delta^{18}O$ (CO_2) = −29 ± 38‰). Although the altitude regions where the isotopes of H_2O and CO_2 were measured with ACS MIR are different (10–50 km for H_2O and 70–130 km for CO_2), which might impede a direct comparison between these, the measurements by SAM/TLS at the surface reported by Webster et al. (2013) also indicate a higher enrichment of H_2O in the heavy isotopes compared to CO_2 ($\delta^{18}O$ (H_2O) = 84 ± 10‰ and $\delta^{18}O$ (CO_2) = 48 ± 5‰).

Based on the equilibrium fractionation of ^{18}O between CO_2 and H_2O derived by Urey (1947) from their different binding energies, Jakosky (1991) suggested that $\delta^{18}O$ should be approximately 80‰ higher in CO_2 than that in H_2O on Mars. This equilibrium could be reached if for example, liquid water was present in the near-surface layer, where CO_2 would be dissolved and would quickly exchange oxygen isotopes with the water. With the liquid water then exchanging with the gases in the atmosphere, the different oxygen-bearing species in the atmosphere would also reflect this equilibrium fractionation (Jakosky, 1991). Although liquid water is unstable under the present Martian conditions, it can be present occasionally as a transient phase (Martín-Torres et al., 2015). However, based on the measured isotope composition in both species, this type of equilibrium does not appear to be dominant in the Martian atmosphere.

Instead, oxygen might be exchanged by photochemical reactions that may ultimately lead to the preferential transfer of certain isotopes to a given species. One pathway by which oxygen is transferred from H_2O to CO_2 starts with the photodissociation of H_2O into OH ($H_2O + h\nu \rightarrow OH + H$). This newly formed odd-hydrogen will later on recombine with CO, giving rise to CO_2 ($CO + OH \rightarrow CO_2 + H$) (McElroy & Donahue, 1972). Based on the differential photolysis cross sections of $H_2^{16}O$ and $H_2^{18}O$ (Miller & Yung, 2000), Alday et al. (2021) estimated that the $^{18}O/^{16}O$ isotopic ratio of the formed OH molecules would be approximately 0.975 times lower than that of the parent H_2O molecules. The recombination of the OH molecules into CO_2 might therefore result in the transfer of oxygen depleted in ^{18}O from H_2O to CO_2.

5. Summary

Transmission spectra acquired by the ACS on the ExoMars TGO allow the monitoring of the C and O isotopic ratios in CO_2 in the atmosphere of Mars. In this study, we develop a retrieval scheme to simultaneously retrieve the isotopic ratios along with the rotational temperature of CO_2, which is found to be essential for an accurate characterization of the isotopic ratios. This retrieval scheme is applied to all ACS MIR observations made with secondary grating position 4 between 70 and 130 km. The observational coverage is divided in two periods, one covering the range L_S = 164–219° in MY34, and the second one covering the range L_S = 141–356° in MY35.

Averaging the retrieved profiles of the isotopic ratios allow the analysis of their altitude trends, which show two main patterns of variations. One pattern comprises an increase in the $^{18}O/^{16}O$ and $^{17}O/^{16}O$ isotopic ratios from 0.9 to 1.0 VSMOW at 70–80 km, to 1.0–1.1 VSMOW at 95–105 km, not followed by the $^{13}C/^{12}C$ ratio. However, a series of tests using synthetic spectra revealed a systematic overestimation of the O isotopic ratios with altitude, consistent with the increase with altitude observed in the data set. Therefore, we conclude that the observed increase in the O isotopic ratios is not caused by real atmospheric fractionation, but by a systematic bias in the retrieval scheme. The second pattern of variations comprise a decrease of the $^{13}C/^{12}C$ and $^{18}O/^{16}O$ isotopic ratios above an altitude of approximately 100 km, which is consistent with the expectations from fractionation above the homopause due to diffusive separation. In particular, fitting the model of this source of fractionation to the vertical trends of the $^{13}C/^{12}C$ ratio reveals a homopause altitude of $z_h = 95 \pm 2$ km, consistent with the values observed in other studies (Slipski et al., 2018).

Making use of the statistics from whole ACS data set, we derive the isotopic ratios representative of CO_2 in the present-day atmospheric reservoir outside of fractionation ($\delta^{13}C = -3 \pm 37‰$; $\delta^{18}O = -29 \pm 38‰$; and $\delta^{17}O = -11 \pm 41‰$). These values differ from those measured by SAM/TLS on the Curiosity Rover (Webster et al., 2013), which were found to be enriched in the heavy isotopes with respect to the standard Earth-like ratios ($\delta^{13}C = 46 \pm 4‰$; $\delta^{18}O = 48 \pm 5‰$; and $\delta^{17}O = 24 \pm 5‰$). To reconcile the measurements from both instruments, we propose two possible scenarios. The first scenario considers the difference between the derived average values to arise from a continuous source of fractionation between the lower and upper atmospheres of Mars, which needs to be accounted for if estimating the escape fractionation factor. In the second scenario, we consider the impact of local isotopic fractionation in the measurements. In that sense, although the measurements made by the SAM/TLS are more precise, they are more constrained in terms of location, season, and local time sampling, where the contribution from climatological fractionation is unknown.

Using the approach of Jakosky (2019), we estimate the amount of C lost to space through time considering the implications of our measurements of the $^{13}C/^{12}C$ ratio. In particular, if considering that the difference between the SAM/TLS and ACS measurements arises from fractionation between the lower and upper atmospheres of Mars, we estimate that at least 40% of the C reservoir on Mars would have been lost to space throughout history. On the other hand, if the C isotopic composition of the present-day atmosphere follows the values derived in this study, we estimate that at least 20% of C would have been lost. These estimates represent a lower limit on the amount of C lost to space since other processes such as outgassing or carbonate formation would produce a relative depletion of the heavy isotopes in the atmosphere.

Finally, we compare the $^{18}O/^{16}O$ isotopic ratio in H_2O ($\delta^{18}O$ (H_2O) $= 140 \pm 80‰$) and CO_2 ($\delta^{18}O$ (CO_2) $= -29 \pm 38‰$), which indicates that the former is more enriched in the heavy isotope. The isotopic ratios in these two species can be different if oxygen is exchanging between them and the isotopes are preferentially transferred to one species over the other. We propose that the enrichment in the heavy isotopes of H_2O over CO_2 might be explained by a transfer of light O from H_2O to CO_2 by photochemical reactions involving the photolysis of these two species, and the posterior recombination of the photolysis products into CO_2.

Appendix A: Validation of the Retrieval Scheme Using Synthetic Spectra

The retrieval scheme presented in this study utilizes a simple description of the radiative transfer calculations, which assume that the gaseous absorption occurs over a homogeneous path with constant pressure and temperature. To analyze the validity and accuracy of this method, a series of retrieval tests are performed using synthetic spectra. The synthetic spectra are generated using the full radiative transfer calculations from the NEMESIS algorithm (Irwin et al., 2008), which split the atmosphere into several layers with different pressure and temperature, and therefore provide a more realistic representation of the atmosphere.

The reference profiles used to generate the synthetic spectra are taken from the Mars Climate Database (MCD; Forget et al., 1999), using the same observational parameters (i.e., latitude, longitude, L_S, and local time) as the ACS MIR observations made during MY34. Since the MCD does not provide atmospheric profiles for the isotopic ratios, these are generated using Equation 5. In particular, we assume random values of the different isotopic ratios below the homopause ($0.7 \leq R_h \leq 1.3$ VPDB or VSMOW), the altitude of the homopause ($90 \leq z_h \leq 110$ km) and the temperature ($100 \leq T \leq 140$ K) for each observation. Using these reference atmospheric profiles for the different species, we generate transmission spectra from 70 to 130 km and add random noise following a

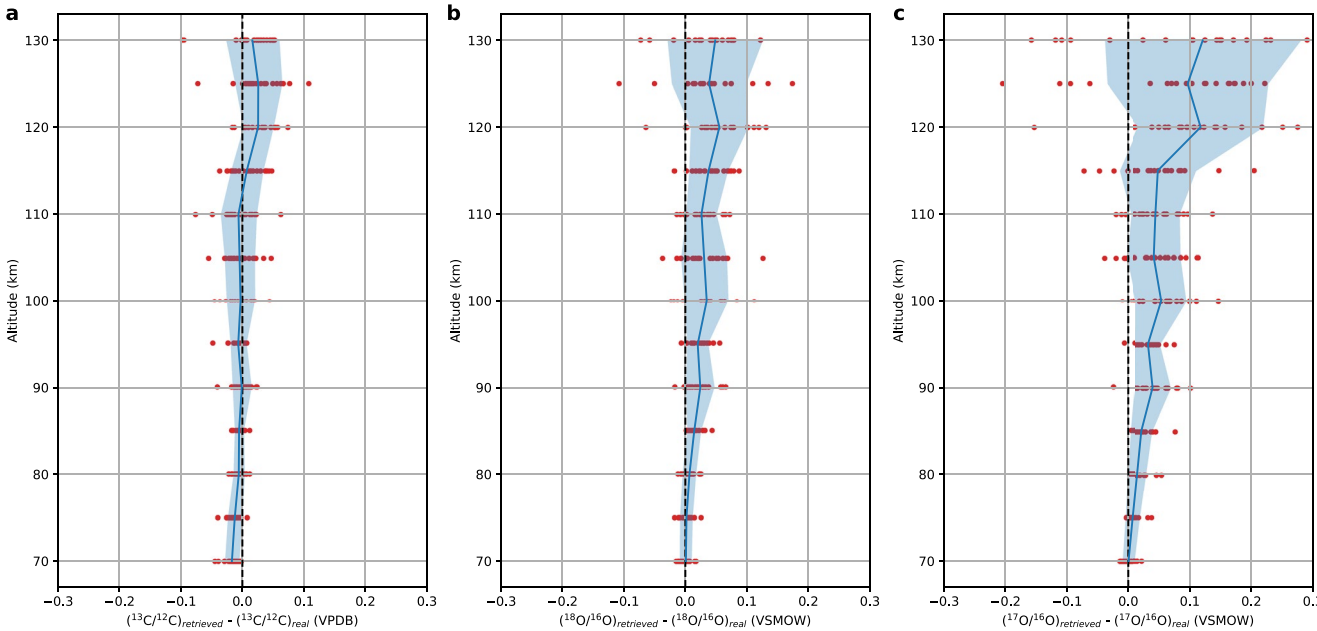

Figure A1. Validation of the retrieval scheme using synthetic spectra. The different panels show the difference between the retrieved $^{13}C/^{12}C$ (a), $^{18}O/^{16}O$ (b) and $^{17}O/^{16}O$ (c) isotopic ratios and the ones that were used to generate the synthetic spectra at each altitude level. The red points represent the values derived from each observation, while the blue lines and shared regions represent the mean and standard deviation of these points at each level. While the mean value of the differences in the $^{13}C/^{12}C$ ratio is close to zero at all altitudes, this quantity reveals a systematic bias in the retrievals of the $^{18}O/^{16}O$ and $^{17}O/^{16}O$ ratios, which tend to overestimate the isotopic ratio.

Gaussian distribution corresponding to a signal-to-noise ratio (SNR) of 5,000, which aim to replicate the ACS MIR measurements.

Once the transmission spectra are generated, these are retrieved using the scheme presented in this study, which assumes a constant pressure and temperature along the path. The results of these retrievals are summarized in Figure A1, which shows the difference between the retrieved isotopic ratios and the ones that were used to generate the synthetic spectra at each altitude for the different observations. In the case that no systematic biases exist, one may expect the average value of these differences to be centered at zero, with some standard deviation representative of the uncertainty of the retrieval. While this is the case for the retrieval of the $^{13}C/^{12}C$ isotopic ratio, Figure A1 suggests a systematic bias in the retrieval of the O isotopic ratios that varies with altitude. In particular, while the convergence between the retrieved and real ratios is good near 70 km, the retrieved isotopic ratios are systematically ∼0.05 VSMOW higher than the ones that were used to generate the synthetic spectra at 100 km. The source of this overestimation of the O isotopic ratios is most likely related to the simplified radiative transfer calculations used in this study. For example, while it is assumed that the temperature field is constant along the path, the averaging kernels shown in Figure 3 indicate that the spectra is sensitive to the layers a few kilometers above the tangent point, which can produce a bias in the retrieved isotopic ratios if there are strong temperature variations along the line of sight. This systematic bias is also expected to occur in the ACS MIR retrievals and might cause an unreal increase of the retrieved isotopic ratios with altitude, which must be taken into account when analyzing the altitude variations of the isotopic ratios.

Data Availability Statement

The data sets generated by the ExoMars Trace Gas Orbiter instruments analyzed in this study are available in the ESA Planetary Science Archive (PSA) repository, https://archives.esac.esa.int/psa/#!Table%20View/ACS=instrument, following a six months prior access period, following the ESA Rules on Information, Data and Intellectual Property. The spectral fitting and retrievals were performed using the NEMESIS radiative transfer and retrieval algorithm (Irwin et al., 2008) and can be downloaded from Irwin (2020). The data products generated in this study (retrieved atmospheric parameters) are available on Alday (2021).

Acknowledgments
The authors thank the reviewers, Timothy A. Livengood and Shohei Aoki, for their useful criticism and suggestions for improvement. The ExoMars mission is a joint mission of the European Space Agency (ESA) and Roscosmos. The ACS experiment is led by the Space Research Institute (IKI) in Moscow, assisted by LATMOS in France. This work was funded by Roscosmos, the National Centre for Space Studies of France (CNES), the Ministry of Science and Education of Russia, the Natural Sciences and Engineering Research Council of Canada (NSERC) (PDF 178 - 516895 - 2018), and the UK Space Agency (ST/T002069/1, ST/R001502/1, and ST/P001572/1).

References

Alday, J. (2021). *Isotopic composition of H_2O and CO_2 on Mars from ACS MIR solar occultations*. Zenodo (Version v01). https://doi.org/10.5281/zenodo.5100449

Alday, J., Trokhimovskiy, A., Irwin, P. G. J., Wilson, C. F., Montmessin, F., Lefévre, F., et al. (2021). Isotopic fractionation of water and its photolytic products in the atmosphere of Mars. *Nature Astronomy*, *5*, 943–950. https://doi.org/10.1038/s41550-021-01389-x

Alday, J., Wilson, C. F., Irwin, P. G. J., Olsen, K. S., Baggio, L., Montmessin, F., et al. (2019). Oxygen isotopic ratios in Martian water vapour observed by ACS MIR on board the ExoMars Trace Gas Orbiter. *Astronomy & Astrophysics*, *630*, A91. https://doi.org/10.1051/0004-6361/201936234

Baker, V. R. (2001). Water and the Martian landscape. *Nature*, *412*(6843), 228–236. https://doi.org/10.1038/35084172

Carr, M. H., & Clow, G. D. (1981). Martian channels and valleys: Their characteristics, distribution, and age. *Icarus*, *48*(1), 91–117. https://doi.org/10.1016/0019-1035(81)90156-1

Cui, J., Wu, X. S., Gu, H., Jiang, F. Y., & Wei, Y. (2019). Photochemical escape of atomic C and N on Mars: Clues from a multi-instrument MAVEN dataset. *Astronomy & Astrophysics*, *621*, A23. https://doi.org/10.1051/0004-6361/201833749

Eiler, J. M., Kitchen, N., & Rahn, T. A. (2000). Experimental constraints on the stable-isotope systematics of CO_2 ice/vapor systems and relevance to the study of Mars. *Geochimica et Cosmochimica Acta*, *64*(4), 733–746. https://doi.org/10.1016/S0016-7037(99)00327-0

Encrenaz, T., Bezard, B., Owen, T., Lebonnois, S., Lefevre, F., Greathouse, T., et al. (2005). Infrared imaging spectroscopy of Mars: H_2O mapping and determination of CO_2 isotopic ratios. *Icarus*, *179*(1), 43–54. https://doi.org/10.1016/j.icarus.2005.06.022

Fedorova, A. A., Montmessin, F., Korablev, O., Luginin, M., Trokhimovskiy, A., Belyaev, D. A., et al. (2020). Stormy water on Mars: The distribution and saturation of atmospheric water during the dusty season. *Science*, *367*(6475), 297–300. https://doi.org/10.1126/science.aay9522

Forget, F., Hourdin, F., Fournier, R., Hourdin, C., Talagrand, O., Collins, M., et al. (1999). Improved general circulation models of the Martian atmosphere from the surface to above 80 km. *Journal of Geophysical Research: Planets*, *104*(E10), 24155–24175. https://doi.org/10.1029/1999JE001025

Fox, J. L., & Bakalian, F. M. (2001). Photochemical escape of atomic carbon from Mars. *Journal of Geophysical Research: Space Physics*, *106*(A12), 28785–28795. https://doi.org/10.1029/2001JA000108

Fox, J. L., & Hać, A. (1999). Velocity distributions of C atoms in CO^+ dissociative recombination: Implications for photochemical escape of C from Mars. *Journal of Geophysical Research: Space Physics*, *104*(A11), 24729–24737. https://doi.org/10.1029/1999JA900330

Gamache, R. R., Roller, C., Lopes, E., Gordon, I. E., Rothman, L. S., Polyansky, O. L., et al. (2017). Total internal partition sums for 166 isotopologues of 51 molecules important in planetary atmospheres: Application to HITRAN2016 and beyond. *Journal of Quantitative Spectroscopy and Radiative Transfer*, *203*, 70–87. https://doi.org/10.1016/j.jqsrt.2017.03.045

Gordon, I., Rothman, L., Hill, C., Kochanov, R., Tan, Y., Bernath, P., et al. (2017). The HITRAN2016 molecular spectroscopic database. *Journal of Quantitative Spectroscopy and Radiative Transfer*, *203*, 3–69. https://doi.org/10.1016/j.jqsrt.2017.06.038

Gröller, H., Lichtenegger, H., Lammer, H., & Shematovich, V. (2014). Hot oxygen and carbon escape from the Martian atmosphere. *Planetary and Space Science*, *98*, 93–105. https://doi.org/10.1016/j.pss.2014.01.007

Hase, F., Wallace, L., McLeod, S. D., Harrison, J. J., & Bernath, P. F. (2010). The ACE-FTS atlas of the infrared solar spectrum. *Journal of Quantitative Spectroscopy and Radiative Transfer*, *111*(4), 521–528. https://doi.org/10.1016/j.jqsrt.2009.10.020

Hu, R., Kass, D. M., Ehlmann, B. L., & Yung, Y. L. (2015). Tracing the fate of carbon and the atmospheric evolution of Mars. *Nature Communications*, *6*(1), 10003. https://doi.org/10.1038/ncomms10003

Irwin, P. (2020). *NEMESIS/Radtrancode Software*. Zenodo. https://doi.org/10.5281/zenodo.4303976

Irwin, P., Teanby, N., de Kok, R., Fletcher, L., Howett, C., Tsang, C., et al. (2008). The NEMESIS planetary atmosphere radiative transfer and retrieval tool. *Journal of Quantitative Spectroscopy and Radiative Transfer*, *109*(6), 1136–1150. https://doi.org/10.1016/j.jqsrt.2007.11.006

Jakosky, B. M. (1991). Mars volatile evolution: Evidence from stable isotopes. *Icarus*, *94*(1), 14–31. https://doi.org/10.1016/0019-1035(91)90138-J

Jakosky, B. M. (1997). Evolution of the Martian atmosphere. *Advances in Space Research*, *19*(8), 1289. https://doi.org/10.1016/S0273-1177(97)83130-4

Jakosky, B. M. (2019). The CO_2 inventory on Mars. *Planetary and Space Science*, *175*, 52–59. https://doi.org/10.1016/j.pss.2019.06.002

Jakosky, B. M., Pepin, R. O., Johnson, R. E., & Fox, J. (1994). Mars Atmospheric loss and isotopic fractionation by solar-wind-induced sputtering and photochemical escape. *Icarus*, *111*(2), 271–288. https://doi.org/10.1006/icar.1994.1145

Jakosky, B. M., Slipski, M., Benna, M., Mahaffy, P., Elrod, M., Yelle, R., et al. (2017). Mars' atmospheric history derived from upper-atmosphere measurements of $^{38}Ar/^{36}Ar$. *Science*, *355*(6332), 1408–1410. https://doi.org/10.1126/science.aai7721

Korablev, O., Montmessin, F., Trokhimovskiy, A., Fedorova, A. A., Shakun, A. V., Grigoriev, A. V., et al. (2018). The atmospheric chemistry suite (ACS) of three spectrometers for the ExoMars 2016 Trace Gas Orbiter. *Space Science Reviews*, *214*(1), 7. https://doi.org/10.1007/s11214-017-0437-6

Krasnopolsky, V. A., Maillard, J. P., Owen, T. C., Toth, R. A., & Smith, M. D. (2007). Oxygen and carbon isotope ratios in the Martian atmosphere. *Icarus*, *192*(2), 396–403. https://doi.org/10.1016/j.icarus.2007.08.013

Krasnopolsky, V. A., Mumma, M., Bjoraker, G., & Jennings, D. (1996). Oxygen and carbon isotope ratios in Martian carbon dioxide: Measurements and implications for atmospheric evolution. *Icarus*, *124*(2), 553–568. https://doi.org/10.1006/icar.1996.0230

Livengood, T. A., Kostiuk, T., Hewagama, T., Smith, R. L., Fast, K. E., Annen, J. N., & Delgado, J. D. (2020). Evidence for diurnally varying enrichment of heavy oxygen in Mars atmosphere. *Icarus*, *335*, 113387. https://doi.org/10.1016/j.icarus.2019.113387

Mahaffy, P. R., Webster, C. R., Atreya, S. K., Franz, H., Wong, M., Conrad, P. G., et al. (2013). Abundance and isotopic composition of gases in the Martian atmosphere from the Curiosity Rover. *Science*, *341*(6143), 263–266. https://doi.org/10.1126/science.1237966

Mahieux, A., Vandaele, A. C., Neefs, E., Robert, S., Wilquet, V., Drummond, R., et al. (2010). Densities and temperatures in the Venus mesosphere and lower thermosphere retrieved from SOIR on board Venus Express: Retrieval technique. *Journal of Geophysical Research*, *115*(E12), E12014. https://doi.org/10.1029/2010JE003589

Martín-Torres, F. J., Zorzano, M.-P., Valentín-Serrano, P., Harri, A.-M., Genzer, M., Kemppinen, O., et al. (2015). Transient liquid water and water activity at Gale crater on Mars. *Nature Geoscience*, *8*(5), 357–361. https://doi.org/10.1038/ngeo2412

McElroy, M. B. (1972). Mars: An evolving atmosphere. *Science*, *175*(4020), 443–445. https://doi.org/10.1126/science.175.4020.443

McElroy, M. B., & Donahue, T. M. (1972). Stability of the Martian atmosphere. *Science*, *177*(4053), 986–988. https://doi.org/10.1126/science.177.4053.986

Miller, C. E., & Yung, Y. L. (2000). Photo-induced isotopic fractionation. *Journal of Geophysical Research: Atmosphere*, *105*(D23), 29039–29051. https://doi.org/10.1029/2000JD900388

Nier, A. O., & McElroy, M. B. (1977). Composition and structure of Mars' Upper atmosphere: Results from the neutral mass spectrometers on Viking 1 and 2. *Journal of Geophysical Research*, *82*(28), 4341–4349. https://doi.org/10.1029/JS082i028p04341

Niles, P. B., Boynton, W. V., Hoffman, J. H., Ming, D. W., & Hamara, D. (2010). Stable isotope measurements of Martian atmospheric CO_2 at the Phoenix landing site. *Science*, *329*(5997), 1334–1337. https://doi.org/10.1126/science.1192863

Niles, P. B., Mahaffy, P. R., Atreya, S., Pavlov, A. A., Trainer, M., Webster, C. R., & Wong, M. (2014). Reconciling the differences between the measurements of CO_2 isotopes by the Phoenix and MSL landers. In *Lunar and Planetary Science Conference* (p. 2573).

Olsen, K. S., Lefèvre, F., Montmessin, F., Fedorova, A. A., Trokhimovskiy, A., Baggio, L., et al. (2021). The vertical structure of CO in the Martian atmosphere from the ExoMars Trace Gas Orbiter. *Nature Geoscience*, *14*, 67–71. https://doi.org/10.1038/s41561-020-00678-w

Olsen, K. S., Toon, G. C., Boone, C. D., & Strong, K. (2016). New temperature and pressure retrieval algorithm for high-resolution infrared solar occultation spectroscopy: Analysis and validation against ACE-FTS and COSMIC. *Atmospheric Measurement Techniques*, *9*(3), 1063–1082. https://doi.org/10.5194/amt-9-1063-2016

Owen, T. (1982). The composition of the Martian atmosphere. *Advances in Space Research*, *2*(2), 75–80. https://doi.org/10.1016/0273-1177(82)90107-7

Owen, T., Biemann, K., Rushneck, D. R., Biller, J. E., Howarth, D. W., & Lafleur, A. L. (1977). The composition of the atmosphere at the surface of Mars. *Journal of Geophysical Research*, *82*(28), 4635–4639. https://doi.org/10.1029/JS082i028p04635

Quémerais, E., Bertaux, J.-L., Korablev, O., Dimarellis, E., Cot, C., Sandel, B. R., & Fussen, D. (2006). Stellar occultations observed by SPICAM on Mars Express. *Journal of Geophysical Research*, *111*(E9), E09S04. https://doi.org/10.1029/2005JE002604

Rahn, T., & Eiler, J. (2001). Experimental constraints on the fractionation of $^{13}C/^{12}C$ and $^{18}O/^{16}O$ ratios due to adsorption of CO_2 on mineral substrates at conditions relevant to the surface of Mars. *Geochimica et Cosmochimica Acta*, *65*(5), 839–846. https://doi.org/10.1016/S0016-7037(00)00592-5

Ramirez, R. M., Kopparapu, R., Zugger, M. E., Robinson, T. D., Freedman, R., & Kasting, J. F. (2014). Warming early Mars with CO_2 and H_2. *Nature Geoscience*, *7*(1), 59–63. https://doi.org/10.1038/ngeo2000

Rodgers, C. D. (2000). *Inverse methods for atmospheric sounding: Theory and practice* (Vol. 2). World Scientific. https://doi.org/10.1142/3171

Schmidt, J. A., Johnson, M. S., & Schinke, R. (2013). Carbon dioxide photolysis from 150 to 210 nm: Singlet and triplet channel dynamics, UV-spectrum, and isotope effects. *Proceedings of the National Academy of Sciences*, *110*(44), 17691–17696. https://doi.org/10.1073/pnas.1213083110

Schrey, U., Rothermel, H., Kaufl, H. U., & Drapatz, S. (1986). Determination of the C-12/C-13 and O-16/O-18 ratio in the Martian atmosphere by 10 micron heterodyne spectroscopy. *Astronomy and Astrophysics*, *155*, 200–204.

Slipski, M., Jakosky, B., Benna, M., Elrod, M., Mahaffy, P., Kass, D., et al. (2018). Variability of Martian turbopause altitudes. *Journal of Geophysical Research: Planets*, *123*(11), 2939–2957. https://doi.org/10.1029/2018JE005704

Urey, H. C. (1947). The thermodynamic properties of isotopic substances. *Journal of the Chemical Society*, 562–581. https://doi.org/10.1039/jr9470000562

Webster, C. R., Mahaffy, P. R., Flesch, G. J., Niles, P. B., Jones, J. H., Leshin, L. A., et al. (2013). Isotope Ratios of H, C, and O in CO_2 and H_2O of the Martian atmosphere. *Science*, *341*(6143), 260–263. https://doi.org/10.1126/science.1237961

Wordsworth, R., Forget, F., Millour, E., Head, J., Madeleine, J.-B., & Charnay, B. (2013). Global modelling of the early Martian climate under a denser CO_2 atmosphere: Water cycle and ice evolution. *Icarus*, *222*(1), 1–19. https://doi.org/10.1016/j.icarus.2012.09.036

Wright, I., Carr, R., & Pillinger, C. (1986). Carbon abundance and isotopic studies of Shergotty and other Shergottite meteorites. *Geochimica et Cosmochimica Acta*, *50*(6), 983–991. https://doi.org/10.1016/0016-7037(86)90379-0

Young, E. D., Galy, A., & Nagahara, H. (2002). Kinetic and equilibrium mass-dependent isotope fractionation laws in nature and their geochemical and cosmochemical significance. *Geochimica et Cosmochimica Acta*, *66*(6), 1095–1104. https://doi.org/10.1016/S0016-7037(01)00832-8